AGU PUBLICATIONS

Geophysical Research Letters

RESEARCH LETTER

10.1002/2014GL059703

Key Points:

- Study both the electrodynamics and thermodynamics of the return stroke channel
- The relationship between the current and optical wave is highly nonlinear
- The current wave speed is significantly higher than the optical wave speed

Correspondence to:
C. Liang,
canliang@stanford.edu

Citation:
Liang, C., B. Carlson, N. Lehtinen, M. Cohen, R. A. Marshall, and U. Inan (2014), Differing current and optical return stroke speeds in lightning, *Geophys. Res. Lett.*, *41*, 2561–2567, doi:10.1002/2014GL059703.

Received 21 FEB 2014
Accepted 10 MAR 2014
Accepted article online 20 MAR 2014
Published online 1 APR 2014

Differing current and optical return stroke speeds in lightning

C. Liang[1], B. Carlson[2,3], N. Lehtinen[1], M. Cohen[4], R. A. Marshall[5], and U. Inan[1,6]

[1]Electrical Engineering, Stanford University, Stanford, California, USA, [2]Department of Physics, Carthage College, Kenosha, Wisconsin, USA, [3]Birkeland Center for Space Science, Bergen, Norway, [4]Electrical and Computer Engineering, Georgia Institute of Technology, Atlanta, Georgia, USA, [5]Aeronautics and Astronautics Department, Stanford University, Stanford, California, USA, [6]Electrical Engineering, Koc University, Istanbul, Turkey

Abstract During the return stroke in downward negative cloud-to-ground lightning, a current wave propagates upward from the ground along the lightning channel. The current wave causes rapid heating of the channel and induces intense optical radiation. The optical radiation wave propagation speed along the channel has been measured to be between $\frac{1}{5}$ and $\frac{2}{3}$ of the speed of light. The current wave speed is commonly assumed to be the same but cannot be directly measured. Past modeling efforts treat either the thermodynamics or electrodynamics. We present the first model that simultaneously treats the coupled current and thermodynamic physics in the return stroke channel. We utilize numerical simulations using realistic high-temperature air plasma properties that self-consistently solve Maxwell's equations coupled with equations of air plasma thermodynamics. The predicted optical radiation wave speed, rise time, and attenuation agree well with observations. The model predicts significantly higher current return stroke speed.

1. Introduction

Lightning consists of many processes spanning a wide range of spatial and time scales, among which the leader-return-stroke sequence takes place outside the cloud and is thus observable by both optical and electromagnetic recording systems. For negative cloud-to-ground lightning, a highly conductive hot plasma channel (hereafter referred to as the "core") is created either by the downward stepped leader for the first return stroke or by a dart leader for the subsequent return stroke. It is generally believed that the core is surrounded by a cold plasma charged region called the "corona sheath," which has very low conductivity and stores the majority of the charge deposited by the leader [*Cooray*, 2006]. A return stroke is initiated once the core makes connection with the ground. A current wave I_{core}, launched at the ground, travels upward along the core, neutralizing the corona sheath charge and causing rapid heating in the core, which in turn induces intense optical radiation. As a result, the current wave is accompanied by a luminous region of the channel extending upward (hereafter referred to as the "optical radiation wave"). A series of observations report the speed of extension of the luminous region, i.e., the optical radiation wave speed v_{opt}, to be between $\frac{1}{5}$ and $\frac{2}{3}$ of the speed of light c [*Idone and Orville*, 1982; *Mach and Rust*, 1989; *Weidman*, 1998; *Wang et al.*, 1999; *Rakov*, 2007b; *Idone et al.*, 1984; *Hubert and Mouget*, 1981]. Direct measurement of the current wave and its propagation speed v_{cur}, however, are not available and must be modeled.

Existing gas-dynamic models apply predefined return stroke current to study the radial dynamics of the core ($\hat{r}$ in Figure 1) [*Rakov and Uman*, 1998]. These models focus on a small segment of the core and solve hydrodynamic equations assuming translational symmetry along the core ($\hat{z}$ in Figure 1). Consequently, they are not suitable for the study of v_{opt} or v_{cur}. Several electromagnetic models calculate I_{core} as a function of both location along the core z and time t, i.e., $I_{\mathrm{core}}(z,t)$ [*Rakov and Uman*, 1998]. However, these models do not explicitly treat the thermodynamic aspect of the physics and thus cannot establish a quantitative connection between $I_{\mathrm{core}}(z,t)$ and the optical radiation power $P_{\mathrm{opt}}(z,t)$.

We present a return stroke model that uses realistic high-temperature air plasma thermodynamic properties and self-consistently solves Maxwell's equations coupled with equations for the dynamics of a high-temperature air plasma. The model assumes a preheated hot plasma core and includes corona sheath effects. We study the behavior of $I_{\mathrm{core}}(z,t)$ and $P_{\mathrm{opt}}(z,t)$ and highlight several features, including the novel physical phenomenon of distinctly different v_{cur} and v_{opt}.

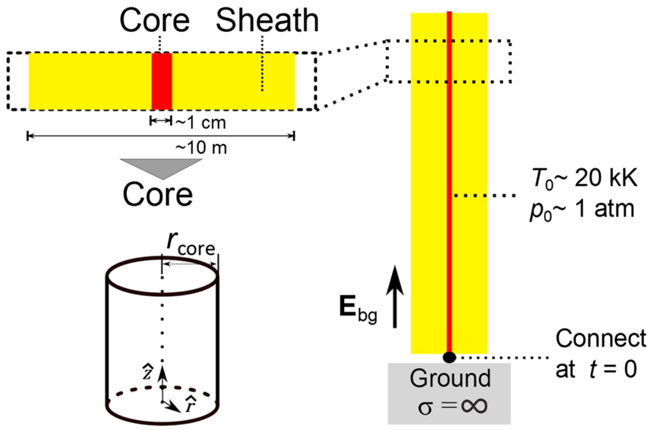

Figure 1. (left) Lightning channel structure: the core and the sheath. (right) The model setup for subsequent return stroke simulation. $\mathbf{E}_{bg}$ is the electric field induced by the cloud and ground charge, t denotes time. T_0 and p_0 are the initial temperature and pressure in the core; $\hat{z}$ is the axial direction (along the core) and $\hat{r}$ the radial direction.

2. Model Construction

2.1. The Core

The core is taken as consisting of two particle systems, namely, the electron gas (e) and the heavy particle gas (O, O^+, N, N^+, etc), with different temperatures T_e, T_h, pressures p_e, p_h, and particle densities n_e, n_h. For the temperature and pressure ranges of interest, negligible error is induced by assuming $p_e = n_e k T_e$ and $p_h = n_h k T_h$ [*D'Angola et al.*, 2008]. Because of the high core temperature ($\geq$20 kK according to *Orville* [1968]) during return stroke, heavy particle excitation and ionization are assumed to be in local thermal equilibrium at T_e. This assumption is verified by simulations for a small segment of the channel using a model that takes into account the finite ionization rate. The simulations show that, because both electron-impact ionization and photon ionization are significant for the temperatures experienced by the core, the heavy particle ionization is kept near or at equilibrium with the electron gas throughout the duration of return stroke. The radial dimension of the conductive portion of the core is specified by r_{core} (Figure 1), and thermodynamic properties are assumed to be radially uniform inside the core. In reality, the core expands during return stroke both due to gas expansion as a result of the pressure rise in the core and due to ionization of ambient air as a result of photon ionization and heat conduction. However, according to gas-dynamic model calculations, r_{core} increases at a speed on the order of 10^3 m s^{-1}, which is many orders of magnitude lower than v_{opt} [*Paxton et al.*, 1986]. This huge speed difference implies that, to the dynamics that determine the current wave and optical wave propagation, r_{core} appears as frozen within a short time window of, for example, $r_{core}/v_{opt} \sim 10^{-10}$ s). In another word, core expansion affects only the quantitative value of $I_{core}(z,t)$ and $P_{opt}(z,t)$ over time scales much longer than 10^{-10} s but not the qualitative relationship between v_{cur} and v_{opt}. Thus, we take the approach of at first assuming r_{core} to be constant and then verifying the conclusion with simulations using different r_{core} values, as well as with simulations that allow r_{core} to increase over time according to a prescribed function. Assuming constant r_{core} is equivalent to neglecting gas expansion in the core and ionization of ambient air next to the core. As a result, the core mass is also a constant. Furthermore, for the temperature and pressure ranges of concern, heavy particles are fully dissociated and thus n_h is also a constant [*D'Angola et al.*, 2008]. For simulations with time varying r_{core}, the core mass and n_h are no longer constants.

To determine the current and charge distribution in the core, we make use of the electric field integral equation (EFIE) and Ohm's Law as in *Miller et al.* [1973] and *Carlson et al.* [2010]. The EFIE provides a physically accurate description of the electric field due to a set of current and charge sources through integration of the time domain Green function to Maxwell's equation [*Jackson*, 1999]. In this case, the integration is taken over the core and the sheath regions. Ohm's Law requires knowledge of the electrical conductivity σ_e. Under the assumptions discussed above, the thermodynamic and transport coefficients of the core, including σ_e, are functions of T_e and n_h. The time variation of T_e and T_h are governed by the energy balance of the two gases (equations (1) and (2)):

$$\left(C_v - \frac{3}{2} k n_h \pi r_{core}^2\right) \frac{d T_e}{dt} = P_{joule} + P_{opt} + P_{e,h} \tag{1}$$

$$\frac{3}{2} k n_h \pi r_{core}^2 \frac{d T_h}{dt} = P_{h,e} - P_{h,air} \tag{2}$$

P_{joule} (W/m) is the per channel length rate of energy gain of electron gas by Joule heating. It is given by $P_{joule} = E_{core} I_{core}$, where E_{core} is the electric field in the axial direction inside the core and I_{core} is dominated by the electron gas flow. The electron gas loses energy by optical radiation P_{opt}, and exchanges energy with the heavy particle gas through elastic collisions $P_{\mathrm{e,h}}$ and heavy particle excitation and ionization. P_{opt} is treated with the approach discussed in *Lowke* [1974] and is a function of T_{e}, n_{h}, and r_{core}. $P_{\mathrm{e,h}}$ is included as in *Zel'dovish and Raizer* [2002]. C_{v} is the constant volume heat capacity per channel length assuming $T_{\mathrm{e}} = T_{\mathrm{h}}$. This term takes heavy particle excitation and ionization into account, as well as the kinetic motion of the electrons and heavy particles. The heavy particle kinetic energy per channel length is given by $\frac{3}{2}kn_{\mathrm{h}}(\pi r_{\mathrm{core}}^2)$, where $n_{\mathrm{h}}(\pi r_{\mathrm{core}}^2)$ is the total number of heavy particles per channel length. With the heavy particle kinetic energy subtracted from C_{v}, the left-hand side of equation (1) represents the internal energy variation with T_{e}.

The heavy particle gas gains energy from $P_{\mathrm{e,h}}$ and loses energy to ambient air $P_{\mathrm{h,air}}$ through heat transfer and gas expansion. The heat transfer is included as in *Bazelyan and Raizer* [1998]. With constant r_{core}, the energy loss due to gas expansion is zero. The error is small because, according to gas dynamic model calculations, this energy loss only accounts for a few percent of the total energy loss [*Paxton et al.*, 1986; *Hill*, 1977]. Moreover, the same conclusions are reached with simulations allowing r_{core} to expand at speeds on the order of 1000 m s^{-1}.

Thermodynamic and transport properties of high-temperature air plasma are involved at various places in the system of equations. For $T_{\mathrm{e}} = T_{\mathrm{h}}$, closed-form expressions for these quantities, with temperature and pressure as the independent variables, are given in *D'Angola et al.* [2008]. For $T_{\mathrm{e}} \neq T_{\mathrm{h}}$, the same expressions can be used with T_{e} as the temperature and a pseudo-pressure p^{s}, defined by equation (3), as the pressure.

$$p^{\mathrm{s}} = (n_{\mathrm{e}} + n_{\mathrm{h}})kT_{\mathrm{e}} \tag{3}$$

This pseudo-pressure is valid because thermodynamic and transport properties are fundamentally only functions of T_{e} and n_{h}. For P_{opt}, p^{s} is taken as the pressure to make use of the results presented in *Aubrecht and Bartlova* [2009].

2.2. The Sheath

Present understanding is insufficient for the construction of a physically accurate model for the sheath. Nevertheless, the main effect of the sheath on the dynamics of the core is the modified electric field in the core, as a result of charge transfer from the core to the sheath. An empirical model that captures this charge redistribution is adequate for the study at hand. Moreover, several measures can be taken to deal with the lack of precise knowledge of the spatial distribution and time evolution of the sheath charge. For example, by choosing the sheath radius r_{sheath} in the model described below, the same electric field in the core associated with the sheath charge can be reproduced as if the correct charge spatial distribution is used. As to the time evolution, we note that, as will be discussed below, the time scale for the charge transfer and temporal variation in sheath charge distribution is on the order of 1 μs. Similar to the expansion of the core discussed in section 2.1, this time scale implies that the temporal evolution of sheath charge does not alter the qualitative relationship between v_{cur} and v_{opt}. Hence, similar simplifications and test procedures are used for the sheath model.

The following empirical model is used (Figure 1). The sheath radius, r_{sheath}, is taken as a constant both along the channel and in time. The sheath charge is assumed to distribute uniformly in the radial direction. The charge transfer rate between the core and the sheath is specified by $I_{\mathrm{c,s}}$:

$$I_{\mathrm{c,s}} = \begin{cases} 0 & \text{if } \lambda_{\mathrm{core}} \leq \lambda_{\mathrm{th}} \\ \frac{\lambda_{\mathrm{core}} - \lambda_{\mathrm{th}}}{\tau_{\mathrm{c,s}}} & \text{if } \lambda_{\mathrm{core}} \geq \lambda_{\mathrm{th}} \end{cases} \tag{4}$$

where $\tau_{\mathrm{c,s}}$ is the relaxation time for excess charge in the core to be carried to the sheath. It is related to the sheath conductivity σ_{sheath}, by $\tau_{\mathrm{c,s}} = \frac{\epsilon_0}{\sigma_{\mathrm{sheath}}}$. λ_{core} is the linear charge density of the core. λ_{th} the threshold linear charge density of the core that can cause air breakdown and is approximately related to the air breakdown voltage E_{th}, by $\lambda_{\mathrm{th}} = 2\pi r_{\mathrm{core}}\epsilon_0 E_{\mathrm{th}}$. According to *Maslowski and Rakov* [2006, 2009], $r_{\mathrm{sheath}} \approx 4$ m and $\tau_{\mathrm{c,s}} \approx 1$ μs. Simulations with different values of the$\tau_{\mathrm{c,s}}$ and r_{sheath} are performed to verify that the conclusion is robust against errors induced by assumptions on the spatial distribution and temporal evolution of sheath charge.

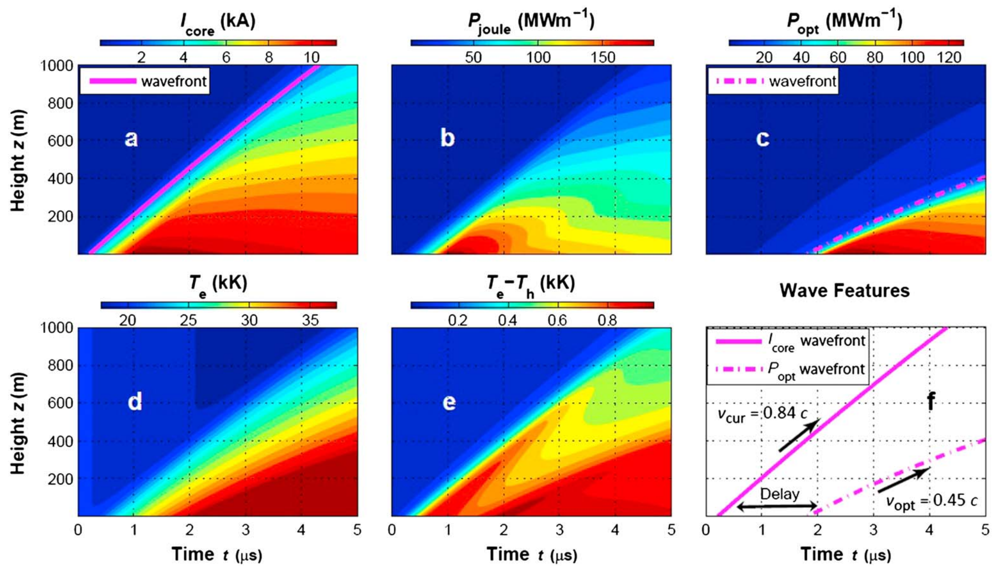

Figure 2. The electrodynamics and thermodynamics of a subsequent return stroke. (a) The return stroke current I_{core}, (b) the joule heating power P_{joule}, (c) the optical radiation power P_{opt}, (d) the electron gas temperature T_e, and (e) the difference between electron gas temperature T_e and heavy particle gas temperature T_h. The simulation parameter values for this simulation are $T_0 = 20$ kK [*Orville*, 1968], $r_{\text{core}} = 4$ mm [*Rakov*, 2007a], $p_0 = 1$ atm [*Rakov and Uman*, 1968], $I^k_{\text{core}} = 12$ kA, $t_{\text{rise}} = 1$ μs, and $t_{\text{fall}} = 30$ μs [*Rakov and Uman*, 2006].

2.3. Simulation Setup

Although the same physical principle applies to both the first return stroke and the subsequent return strokes, it is convenient to focus on the subsequent return stroke, because the thermodynamic properties of the core created by dart leader processes vary more smoothly along the channel. The model configuration for the subsequent return stroke simulation is shown in Figure 1. While the channel in the model follows a straight line, real lightning channel is tortuous. However, *Hill* [1968] shows that the average angle of change in channel direction is less than 20°, and thus the error in the channel length representation is less than 6%. For $t < 0$, the channel is disconnected from the ground. The core and sheath charge are allowed to redistribute until no current flows in the core. At $t = 0$, the channel is connected to the ground. T_e, T_h, p_e, and p_h are set to their initial values. Because the physics of the current and optical radiation wave propagation along the core is independent of how the current is initiated at the ground, the return stroke current at ground, $I_{\text{core}}(z = 0, t)$, is treated as an external source and is specified using equation (5), as in *Plooster* [1971].

$$I_{\text{core}}(z = 0, t) = I^k_{\text{core}} \begin{cases} 0 & \text{if } t \le 0 \\ \frac{t}{\tau_{\text{rise}}} & \text{if } 0 \le t \le \tau_{\text{rise}} \\ \exp\left(-\frac{t-\tau_{\text{rise}}}{\tau_{\text{fall}}}\right) & \text{if } t \ge \tau_{\text{rise}} \end{cases} \tag{5}$$

where τ_{rise}, τ_{fall}, and I^k_{core} are the rise time, fall time, and peak current, respectively. The resulting waveform is representative of experimental recordings [*Berger et al.*, 1975]. The ground is assumed to have infinite conductivity and treated with the method of images. Since the cloud charge distribution varies over a time scale much longer than the time frame of concern, its associated electric field is directly specified as $\mathbf{E}_{\text{bg}}$ and is assumed to be time invariant. For the numerical computation, both the core and the sheath are discredited along the channel into 3 m long segments, with the time step equal to 10^{-8} s. The results show negligible difference from simulations with smaller grid sizes.

3. Results and Discussion

We first examine the simulation result for a single return stroke (Figure 2). The temporal and spatial evolution of I_{core} and P_{opt} are shown in Figures 2a and 2c, respectively. The optical radiation wavefront highlighted in Figure 2c corresponds to the time when, at each altitude z, $P_{\text{opt}}(z, t)$ reaches 20% of its peak value at

10.1002/2014GL059703

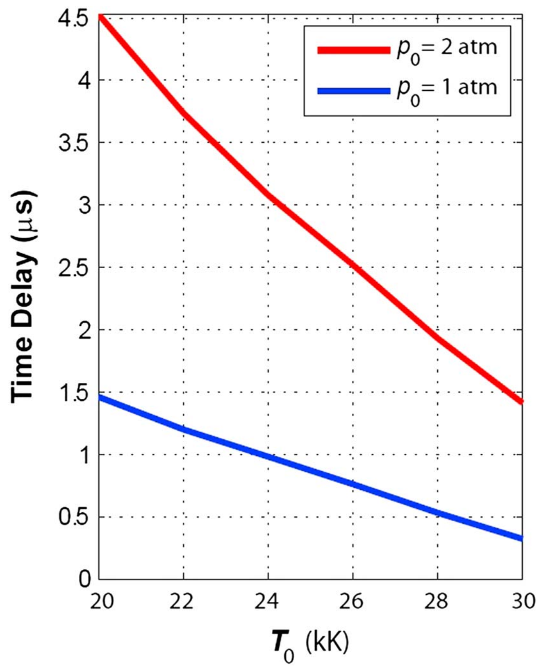

Figure 3. The time delay of peak P_{opt} relative to peak I_{core} at ground as a function of the initial channel temperature T_0 for initial pressure $p_0 = 1, 2$ atm. With respect to the speed of light c, v_{cur}, and v_{opt} are normalized. For all the simulation presented, $p_0 = 1$ atm, $r_{core} = 4$ mm, $I^k_{core} = 12$ kA, $t_{rise} = 1$ μs, and $t_{fall} = 30$ μs.

the ground ($z = 0$). In this case, v_{opt} is the slope of the wavefront and is approximately 0.45 c. This definition of wavefront and wave speed is consistent with the technique used to measure optical return stroke speed from streak camera recordings [*Idone and Orville*, 1982]. Applying the same definition of wavefront to $I_{core}(z,t)$, v_{cur} is found to be approximately 0.84 c. Figure 2f shows a comparison of the wavefronts, which reveals a finite time delay between them.

Both waves experience attenuation and dispersion as they propagate along the core. For example, by fitting an exponential decay curve to $\max_t P_{opt}(z,t)$, the height decay constant is found to be approximately 0.6 km, in agreement with *Jordan and Uman* [1983]. The 10–90% rise time of $P_{opt}(z,t)$, is 0.71 μs for $z = 30$ m and 2.3 μs for $z = 300$ m, in agreement with *Wang et al.* [1999]. In contrast, the height decay constant for $\max_t I_{core}(z,t)$ is approximately 1.05 km. The 10–90% rise time of $I_{core}(z,t)$, is 0.80 μs for $z = 30$ m and 0.9 μs for $z = 300$ m.

Analysis of P_{joule} (Figure 2b) and T_e (Figure 2d) offers further insight into the underlying dynamics. Because of the dispersion and attenuation in the current wave, $P_{joule}(z,t)$ decreases with z (Figure 2b) and so does the heating rate of the core (Figure 2d). On the other hand, P_{opt} is a highly nonlinear function of T_e and thus the wavefront of P_{opt} corresponds to a T_e that is much greater than the initial temperature ($T_e \approx 32$ kK at the optical radiation wavefront for the simulation shown). The lower heating rate at higher altitude means that longer time is required for the core to reach such a high temperature. As a result, the optical radiation wavefront is further delayed with respect to the current wavefront at higher altitude, hence the lower v_{opt} than v_{cur}.

The delay of the optical radiation wave relative to the current wave also varies appreciably with initial conditions of the core. For example, Figure 3 shows the increase in the time delay between the peak I_{core} and peak P_{opt} at the ground with decreasing initial temperature. Further experiments with rocket-triggered lightning that look into the time delay between channel base current and optical emissions may be used to further narrow down the initial condition of the core near ground. Also, note that for real return stroke, the core initial temperature is expected to be lower at higher altitudes, and thus the delay of the optical radiation wave with respect to the current wave is expected to be further enlarged. As a result, v_{opt} could be further reduced relative to v_{cur}.

In Figure 2d, the maximum T_e at ground is approximately 38 kK, reasonably close to the estimated maximum temperature of 36 kK based on spectroscopic observations [*Orville*, 1968], although the spectroscopic observations have a limited time resolution (∼2 to 5 μs) that may reduce the true maximum. The maximum n_e is approximately 8×10^{23} m^{-3}, in reasonable agreement with *Orville* [1968]. As to $T_e - T_h$, it is significant initially, reaching beyond 1 kK in approximately 2 μs after the current wave arrives but quickly decreases to nearly zero within a few microseconds (Figure 2e), in agreement with gas dynamics model studies [*Paxton et al.*, 1986].

Figure 4 presents v_{cur} (dash lines) and v_{opt} (solid lines) for a series of simulations using different values of r_{core} and I^k_{core}. The shaded areas indicate the variation in v_{opt} as the threshold used to identify optical radiation wavefront is varied from 15% to 25% of the maximum $P_{opt}(z,t)$ at $z = 0$. v_{cur} varies much less with the choice of threshold. After excluding the contribution from the factor above, the dependence of v_{opt} on r_{core} is still very strong. This dependence is a result of the highly nonlinear dependence of P_{opt} on r_{core} [*Aubrecht and Bartlova*, 2009]. On one hand, the strong dependence suggests that precise calculation of v_{opt} requires

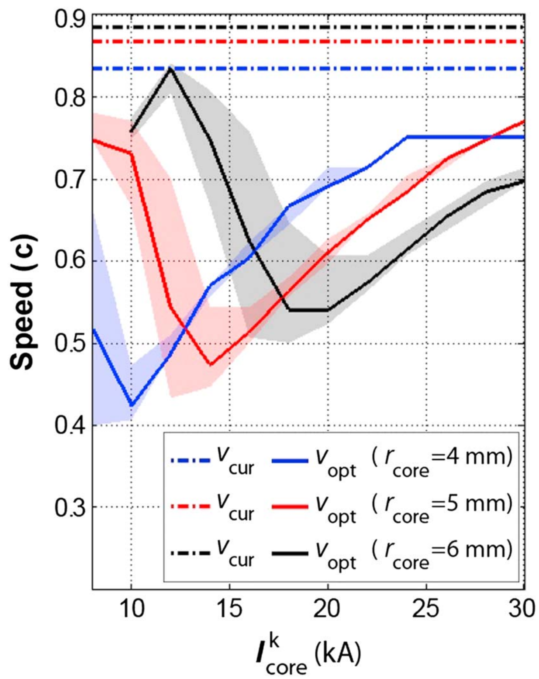

Figure 4. The variation of v_{opt} and v_{cur} with r_{core} and I^k_{core}. v_{cur} and v_{opt} are normalized with respect to the speed of light c. For all the simulations presented, T_0=20 kK, $p_0 = 1$ atm, $t_{rise} = 1$ µs, and $t_{fall} = 30$ µs. The shaded areas indicate the variation in v_{opt} as the threshold used to identify optical radiation wavefront is varied from 15% to 25% of the maximum $P_{opt}(z, t)$ at $z = 0$. v_{opt} for $r_{core} = 6$ mm and $I^k_{core} < 10$ kK is not shown, because in these cases 20% of the maximum optical power at ground is less than the initial optical power and thus the definition does not apply.

improved treatment of the radial dynamics of the core and more accurate knowledge of the initial condition of the core. On the other hand, v_{cur} being consistently higher than v_{opt} for a wide range of parameter values and for simulations that allow r_{core} to expand according to predefined functions confirms that the relationship is robust against the errors associated with model assumptions of the core. Also, note that the large variation in v_{opt} given I^k_{core} may partially explain the absence of correlation between I^k_{core} and v_{opt} as observed by *Mach and Rust* [1989]. In contrast, v_{cur} appears to be independent on I^k_{core}. This independence indicates that $I_{core}(z, t)$ scales approximately linearly with I^k_{core}, despite the nonlinear dependence of σ_e on T_e and in turn on I^k_{core}. This is because, with $T_e \geq 20$ kK, the core remains highly conductive for the entire duration of return stroke. However, the linearity no longer holds in the presence of core expansion. Similar tests are performed for the other model parameters, and in all cases v_{cur} is consistently higher than v_{opt}, confirming that the relationship is unaffected by errors associated with the model assumptions.

As shown by *Krider* [1992] and *Thottappillil et al.* [2001, 2004, 2007], the higher v_{cur} has profound effect on the calculated return stroke electromagnetic radiation. For example, calculation of the electric field 100 km away from return stroke channel base as presented by *Thottappillil and Rakov* [2007] shows that, as v_{cur} increases from 0.5c to c, the field angular distribution becomes more focused toward the vertical direction above the channel and the field peak amplitude rapidly increases by over an order of magnitude. The higher peak electric field directly leads to a higher probability of initiation for transient luminous effects in the mesosphere, while the field angular distribution may affect the geometrical appearance of these phenomena. Generally speaking, the relationship $v_{cur} > v_{opt}$ is important for lightning geolocation [*Cummins et al.*, 1998] and lightning-upper atmosphere coupling applications [*Cummer et al.*, 1998], for which the electromagnetic pulse radiated from lightning has been derived by assuming $v_{cur} = v_{opt}$. It is also of interest to note that, based on comparison between the calculated and experimentally observed electromagnetic field near return stroke channel, *Thottappillil et al.* [2001] suggest the possibility of $v_{cur} \approx c$ near the bottom of the channel.

4. Summary

We have presented a model that can be used to study the highly nonlinear interaction between the electrodynamics and the thermodynamics of the core. The model captures a wide range of observed return stroke features and, in particular, correctly predicts v_{opt} to fall between $\frac{1}{5}c$ and $\frac{2}{3}c$. The model also predicts a much higher v_{cur} than v_{opt} and a finite time delay of the optical radiation wave relative to the current wave. Various tests suggest that these predictions hold true for a wide range of physical parameters and in the presence of core expansion.

Acknowledgments
This work was supported by Defense Advanced Research Projects Agency grant agreement HR0011-10-1-0058, the European Research Council under the European Union's Seventh Framework Programme (FP7/2007-2013)/ERC grant agreement 320839, and the Research Council of Norway under contracts 208028/F50, 216872/F50 (CoE).

The Editor thanks Rajeev Thottappillil and an anonymous reviewer for their assistance in evaluating this paper.

References

Aubrecht, V., and M. Bartlova (2009), Net emission coefficients of radiation in air and SF6 thermal plasmas, *Plasma Chem. Plasma Process.*, *29*, 131–147.
Bazelyan, E. M., and Y. P. Raizer (1998), *Spark Discharge*, 38–42, CRC Press, Boca Raton, Fla.
Berger, K., R. B. Anderson, and H. Kroninger (1975), Parameters of lightning flashes, *Electra*, *41*, 23–37.

Carlson, B. E., N. G. Lehtinen, and U. S. Inan (2010), Terrestrial gamma ray flash production by active lightning leader channels, *J. Geophys. Res.*, *115*, A10324, doi:10.1029/2010JA015647.

Cooray, V. (2006), *The Lightning Flash*, pp. 144–145, Cambridge Univ. Press, Cambridge, U. K.

Cummins, K. L., E. P. Krider, and M. D. Malone (1998), The U.S. National Lightning Detection Network and applications of cloud-to-ground lightning data by electric power utilities, *IEEE Trans. Electromagn. Compat.*, *40*(II), 465–80.

Cummer, S. A., U. S. Inan, and T. F. Bell (1998), Ionospheric *D* region remote sensing using VLF radio atmospherics, *Radio Sci.*, *33*, 1781–1792.

D'Angola, A., G. Colonna, C. Gorse, and M. Capitelli (2008), Thermodynamic and transport properties in equilibrium air plasmas in a wide pressure and temperature range, *Eur. Phys. J. D*, *46*, 129–150.

Krider, E. P. (1992), On the electromagnetic fields, Poynting vector, and peak power radiated by lightning return strokes, *J. Geophys. Res.*, *97*, 15,913–15,917.

Hill, R. D. (1968), Analysis of irregular paths of lightning channels, *J. Geophys. Res*, *73*, 1897–1906.

Hill, R. D. (1977), Energy dissipation in lightning, *J. Geophys. Res*, *82*, 4967–4968.

Hubert, P., and G. Mouget (1981), Return stroke velocity measurements in two triggered lightning flashes, *J. Geophys. Res.*, *86*, 5253–5261.

Idone, V. P., and R. E. Orville (1982), Lightning return stroke velocities in the Thunderstorm Research International Program (TRIP), *J. Geophys. Res.*, *87*, 4903–4915.

Idone, V. P., R. E. Orville, P. Hubert, L. Barret, and A. Eybert-Berard (1984), Correlated observations of three triggered lightning flashes, *J. Geophys. Res.*, *89*, 1385–94.

Jackson, J. D. (1999), *Classical Electrodynamics*, pp. 243–247, 3rd ed, John Wiley, Hoboken, N. J.

Jordan, D. M., and M. A. Uman (1983), Variation in light intensity with height and time from subsequent lightning return strokes, *J. Geophys. Res*, *88*, 6555–6562.

Lowke, J. J. (1974), Predictions of arc temperature profiles using approximate emission coefficients for radiation losses, *J. Quant. Spectrosc. Radiat. Transfer*, *14*, 111–122.

Miller, E. K., A. J. Poggio, and G. J. Burke (1973), An intergro-differential equation technique for the time-domian analysis of thin wire structures. 1. The numerical method, *J. Comput. Phys.*, *12*, 24–48.

Mach, D. M., and W. D. Rust (1989), Photoelectric return-stroke velocity and peak current estimates in natural and triggered lightning, *J. Geophys. Res.*, *94*, 6159–6164.

Maslowski, G., and V. A. Rakov (2006), A study of the lightning channel corona sheath, *J. Geophys. Res.*, *111*, D14110, doi:10.1029/2005JD006858.

Maslowski, G., and V. A. Rakov (2009), Dynamics of lightning channel corona sheath predicted by return-stroke models with specified longitudinal current distribution, *Publs. Inst. Geophys. Pol. Acad. Sc.*, *D-73*(412), 89–98.

Orville, R. E. (1968), A high-seed time-resolved spectroscopic study of the lightning return stroke: Part 2. A quantitative analysis, *J. Atmos. Sci.*, *25*, 839–851.

Paxton, A. H., R. L. Gardner, and L. Baker (1986), Lightning return stroke. A numerical calculation of the optical radiation, *Phys. Fluids*, *29*, 2736–2741.

Plooster, M. N. (1971), Numerical model of the return stroke of the lightning discharge, *Phys. Fluids*, *14*, 2124–2133.

Rakov, V. A. (2007a), Some inferences on the propagation mechanism of dart leaders and return strokes, *J. Lightning Res.*, *1*, 80–89.

Rakov, V. A. (2007b), Lightning return stroke speed, *J. Lightning Res.*, *1*, 80–89.

Rakov, V. A., and M. A. Uman (1998), Review and evaluation of lightning return stroke models including some aspects of their application, *IEEE Trans. Electromagn. Compat.*, *40*, 403–426.

Rakov, V. A., and M. Uman (2006), *Lightning: Physics and Effects*, 143–164, Cambridge Univ. Press, Cambridge, U. K.

Rakov, V. A., and M. Uman (1968), Time interval between lightning strokes and the initiation of dart leaders, *J. Geophys. Res.*, *73*, 497–506.

Thottappillil, R., J. Schoene, and M. A. Uman (2001), Return stroke transmission line model for stroke speed near and equal that of light, *Geophys. Res. Lett.*, *28*, 3593–3596.

Thottappillil, R., M. A. Uman, and N. Theethayi (2004), Electric and magnetic fields from a semi-infinite antenna above a conducting plane, *J. Electrostat.*, *61*, 209–221.

Thottappillil, R., and V. A. Rakov (2007), Review of three equivalent approaches for computing electromagnetic fields from an extending lightning discharge, *J. Lightning Res.*, *1*, 90–110.

Wang, D., N. Takagi, and T. Watanab (1999), Observed leader and return-stroke propagation characteristics in the bottom 400 in of a rocket-triggered lightning channel, *J. Geophys. Res.*, *104*, 14,369–14,376.

Weidman, C. D. (1998), Lightning return stroke speed near channel base, *Proceedings of the 1998 International Lightning Detection Conference, Tucson, Ariz., U.S.A, 25*.

Zel'dovish, Y. B., and Y. P. Raizer (2002), *Physics of Shock Waves and High-Temperature Hydrodynamic Phenomena*, pp. 420–421, Dover Publications, Inc., New York.

